Chinese Chemical Letters 34 (2023) 107833

Contents lists available at ScienceDirect

Chinese Chemical Letters

journal homepage: www.elsevier.com/locate/cclet

Machine learning accelerated DFT research on platinum-modified amorphous alloy surface catalysts

Xi Zhang[a,b,c,*], Kangpu Li[a], Bo Wen[a,c], Jiang Ma[b], Dongfeng Diao[a]

[a] Institute of Nanosurface Science and Engineering, Guangdong Provincial Key Laboratory of Micro/Nano, Shenzhen University, Shenzhen 518060, China
[b] College of Mechatronics and Control Engineering, Shenzhen University, Shenzhen 518060, China
[c] Research Center of Medical Plasma Technology, Shenzhen University, Shenzhen 518060, China

ARTICLE INFO

Article history:
Received 24 June 2022
Revised 29 August 2022
Accepted 14 September 2022
Available online 17 September 2022

Keywords:
Hydrogen evolution reaction
Amorphous alloy
Density functional theory
Machine learning

ABSTRACT

Pt-modified amorphous alloy (Pt@PdNiCuP) catalyst exhibits excellent electro-catalytic activity and high experimental durability for hydrogen evolution reaction (HER). However, the physical origin of the catalytically active remains unclear. In this paper, we constructed a distance contribution descriptor (DCD) for the feature engineering of machine learning (ML) potential, and calculated the Gibbs free energies (ΔG_H) of 46,000 *H binding sites on the Pt@PdNiCuP surface by ML-accelerated density functional theory (DFT). The relationship between ΔG_H and DCD revealed that in the H-Pt distance region of 2.0–2.5 Å where the parabolic tail and disordered scatters coexist, the H-metal bonding configuration is mainly the bridge- or hollow- bonding type. The contribution analysis of DCD indicates that the joint effect of Pt, Pd and Ni atoms determines the catalytical behavior of amorphous alloy, which agrees well with experimental results. By counting atomic percentages in different energy intervals, we obtained the atomic ratio for the best catalytic performance (Pt:Pd:Ni:Cu:P = 0.33:0.17:0.155:0.16:0.185). Projected density of states (PDOS) show that H 1s orbital, Pt 5d orbital, and Pd 4d orbital form a bonding state at −2 eV. These results provide new ideas for designing more active amorphous alloy catalysts.

Hydrogen is considered as one of the most ideal alternative energy sources for fossil fuels due to its carbon-free, clean and efficient, and abundant natural resources [1]. Currently, a promising and economical strategy is electrochemical water splitting or hydrogen evolution reaction to produce hydrogen [2–4]. The development of efficient and durable electro-catalysts is crucial for the HER. Pt-based materials have been found to be the most efficient catalysts for HER, but the high cost and scarcity of Pt limit its commercial application. The synergy between the elements of amorphous alloys or metallic glasses and a large number of incongruent sites on the surface provide the possibility for the design of efficient HER catalyst. In recent years, including Pd- [5], Fe- [6], Al- [7], Ni- [8] and Co-based [9] amorphous alloy catalysts for HER have been extensively studied. Unfortunately, they still fall short of the high activity and durability of Pt-based alloys. So far, Pt-based materials are still the most efficient HER catalysts. To reduce the use of Pt, one strategy is to intercalate Pt onto the surface of amorphous alloys. Our previous results show experimentally that Pt@PdNiCuP has the best Tafel coefficient among all the catalysts obtained and unexpected self-stabilized performance in HER processes (the number of sites is about 3 times that of Pt/C, and no degradation occurs for 500 h at an overpotential of 200 mV) [10]. However, limited by experimental conditions and cost, the relationship between the catalytic activity of Pt@amorphous alloys and the local atomic environment is still not effectively resolved.

Density functional theory (DFT) has been shown to be a promising strategy for calculating adsorption energies and catalyst atomic design [11–14], but its high computational cost and computational complexity limit its application in exploring catalytic properties. In recent years, computationally efficient and data-driven machine learning models (ML) have shown great potential in accelerating the development of catalytic technologies, which incorporate data sets containing chemical information as an effective tool for researchers [15–23]. Several research groups have successfully combined density functional theory with machine learning to reveal some interesting discoveries in amorphous alloy or high-entropy alloy catalysts. Batchelor *et al.* used DFT combined with the least-squares algorithm to predict the adsorption energy of IrPdPtRhRu and reaction intermediates well [24]. Mao *et al.* proposed an effective high-throughput HER catalyst screening strategy through high-throughput DFT calculation combined with a neural network

* Corresponding author at: Institute of Nanosurface Science and Engineering, Guangdong Provincial Key Laboratory of Micro/Nano, Shenzhen University, Shenzhen 518060, China.
E-mail address: zh0005xi@szu.edu.cn (X. Zhang).

https://doi.org/10.1016/j.cclet.2022.107833
1001-8417/

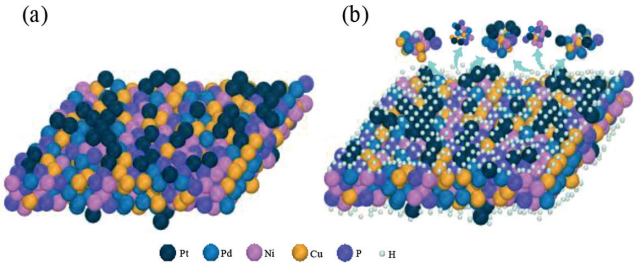

Fig. 1. (a) $Pt_{84}@Pd_{140}Ni_{140}Cu_{140}P_{140}$ model after geometric optimization. (b) Schematic diagram of sampling the H atom adsorption site.

model [25]. Saidi *et al.* developed a method based on machine learning and global optimization to optimize the activity of CoMoFeNiCu for ammonia decomposition and ammonia synthesis [26]. These works mainly study the catalytic performance in a relatively limited local atomic environment, and the research on the ligand diversity and coordination complexity of amorphous materials is still rarely covered.

In this paper, DFT calculations combined with ML models were used to predict the ΔG_H of adsorption sites under different ligands and coordination of amorphous alloys (Pt@PdNiCuP), which provides conditions for the study of catalytic performance. We sampled 46,000 adsorption sites on the Pt@PdNiCuP surface and construct distance contribution descriptors (DCD) to provide an efficient dataset for machine learning models. Through statistical analysis, the influence mechanism of each element on catalytic activity was clarified from the perspective of atomic distance and atomic percentage, and the atomic ratio with the best catalytic performance was predicted. In addition, we also calculated the charge density difference and projected density of states (PDOS) to investigate the mechanism by which the local atomic environment affects the catalytic activity. These results provide new ideas for designing more active amorphous alloy catalysts.

The algorithm consists of three parts (Fig. S1 in Supporting information): (1) The stochastical generation of the local atomic environment and accurate DFT-level Gibbs free energy calculations for 920 H adsorption sites on the surface of Pt@PdNiCuP; (2) Using distance contribution descriptors (DCD) perform feature extraction, divide the data into the training set and test set, train machine learning potential and evaluate the performance of machine learning potential respectively; (3) 46,000 adsorption sites were densely sampled on the two surfaces of Pt@PdNiCuP, the ΔG_H of the adsorption sites were predicted, and finally, the results were statistically analyzed.

We adopted the Pd supercell in which both surfaces are the energetically favored (111) facet [27,28]. We construct a Pd atomic supercell of $14 \times 10 \times 4$ with a total atom of 560 and randomly changed the atomic composition according to the atomic ratio, thereby obtaining the substrate $Pd_{140}Ni_{140}Cu_{140}P_{140}$. Then Pt atoms were randomly inserted on both sides of the substrate according to the ratio, and finally, the structure of $Pt_{84}@Pd_{140}Ni_{140}Cu_{140}P_{140}$ was obtained (644 atoms). 20 Å vacuum layer was added along the Z-axis to avoid dipole–dipole interactions. To obtain a stable atomic structure, we performed DFT structure optimization on $Pt_{84}@Pd_{140}Ni_{140}Cu_{140}$ P_{140}, and the results are shown in Fig. 1a. All DFT calculations are performed using the Vienna ab initio simulation package (VASP) (see Supporting information for full details) [29,30].

It is well known that the ΔG_H of H adsorption is often used as an indicator of HER activity [31–33]. To maintain high catalytic activity, H atoms should not bind too strongly or too weakly to the catalyst surface, so that both adsorption and desorption are fast. This requirement indicates that the catalyst has high activity for the HER when the ΔG_H of adsorbed H atoms is around 0 eV [34,35]. The formula for calculating the ΔG_H of H adsorption site is as follows:

$$\Delta G_H = \Delta E_H - \Delta E_{ZPE} - T\Delta S_H \quad (1)$$

where ΔG_H represents the H adsorption energy, ΔE_{ZPE} and ΔS_H are the zero-point energy (ZPE) and the entropy between the H adsorption state and the gas phase, respectively. ΔE_H is defined as:

$$\Delta E_H = E_{H+MG} - E_{MG} - \left(\frac{1}{2}\right)E(H_2) \quad (2)$$

where E_{H+MG} is the total energy of H atoms adsorbed on the surface of the Pt@PdNiCuP, E_{MG} is the energy of the Pt@PdNiCuP, and $E(H_2)$ is the energy of H_2. The energy of H_2 is −6.97 eV. As the vibrational entropy of H atom can be ignored, that is, $\Delta S_H \approx (1/2)\Delta S(H_2)$. Hence, the ΔG_H can be simplified to $\Delta G_H = \Delta E_H + 0.24$ eV.

The catalytic performance of amorphous alloys is closely related to the local atomic environment. To obtain the H atom adsorption sites under different ligands and coordination environments on the catalyst surface, we took an average of 460 sampling points on the upper and lower surfaces of $Pt_{84}@Pd_{140}Ni_{140}Cu_{140}P_{140}$ to obtain a rich local atomic environment, as shown in Fig. 1b. After determining the X, Y coordinates of the H atom, set its position as the center of the circle and extract the Z coordinate of the highest atom in a circular area with a radius 2.0 Å. Then randomly add 0.8–1.8 Å to the Z coordinate of the highest atom to obtain the height of the H atom along the Z-direction. When the spatial position of the H atom is determined, the atomic cluster in the spherical area with the H atom as the center and the radius of 5.0 Å is extracted, which is the local atomic environment that affects the adsorption performance of the active site. The original dataset was established by DFT calculations and the ΔG_H of 920 adsorption sites was obtained.

To construct data for machine learning, we need to convert the obtained raw data (atomic structure) into features for machine learning through data descriptors. The ΔG_H of the H atom adsorption site is closely related to the "ligand effect" and "coordination effect" of H atom adsorption [36]. To construct a feature that can approximately reflect the coordination and ligand states of H atom adsorption sites, we constructed a distance contribution descriptor (DCD) to describe the coordination of H atoms in the local atomic environment, which is defined as:

$$DCD = \frac{1}{D_{H-X}^m}, \ m = 1, \ 2, \ 3, \ldots, n \quad (3)$$

where $D_{H\text{-}X}$ represents the H-metal (Pt, Pd, ...) distance, X = {Pt, Pd, Ni, Cu, P}.

Next, we combined the contribution of the distance between the H atom and each atom in the local environment in order according to the element type, and finally obtained the characteristic that can approximately reflect the coordination and ligand state of the H atom adsorption site: $[\frac{1}{D_{H-Pt}^m}; \frac{1}{D_{H-Pd}^m}; \frac{1}{D_{H-Ni}^m}; \frac{1}{D_{H-Cu}^m}; \frac{1}{D_{H-P}^m}]$, the feature data extraction process is shown in Fig. 2. The characteristics are controlled by two factors: the first is the contribution value of the distance between atoms, and the second is the number of atoms of each element, which together describe the state of the coordination and ligand of the H atom in the local atomic environment. In general, the features we constructed consist of simple geometric elements, which can effectively transform the atomic structure of the adsorption site into data for machine learning. The representative feature data set is shown in Tables S1 (Supporting information).

To determine the power m of the DCD, we use the performance of the machine learning model as the evaluation standard to select

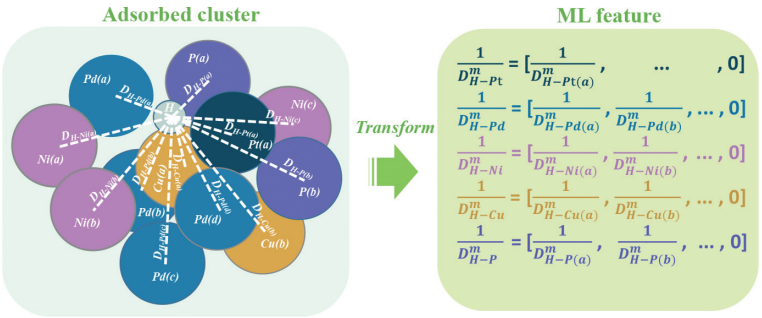

Fig. 2. Schematic diagram of H atom adsorption cluster features data extraction.

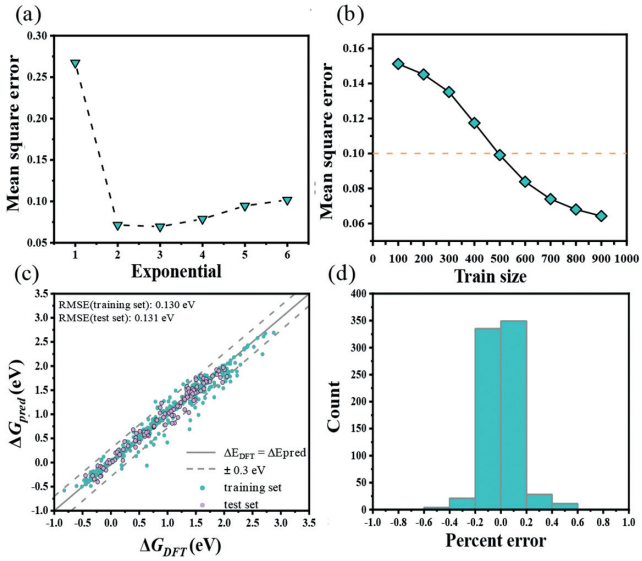

Fig. 3. (a) Mean square error of different features. (b) The variation of the mean square error versus train set size. (c) The SVR model is trained on a training set of 800 samples and tested on a test set of 100. The solid line is the ideal ratio of DFT energy to predicted energy of 1:1. (d) The relative error percentage distribution on 800 samples.

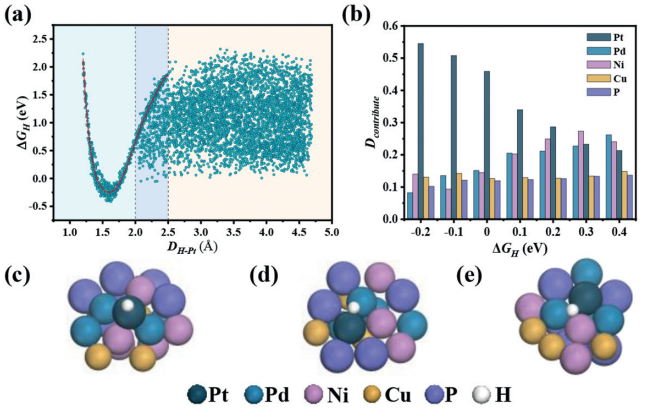

Fig. 4. Atomic environment of H-metal distance. (a) The relationship between the H–Pt distance and the ΔG_H (the solid red line is the result of polynomial fitting); (b) H-metal distance contribution analysis as the function of ΔG_H; Illustration of (c) on-site configuration of H–Pt bonding, (d) bridge configuration of Pt–H–Pd bonding, (e) hollow configuration of H–Pt–Pd–Ni bonding.

the optimal power m of the DCD. The machine learning model is developed using scikit-learn code [37]. The code for training the model is based on Python 3.8.5 (see Supporting information for full details). Based on this, we select $m = 1$, 2, 3, 4, 5 and 6 to train the support vector regression (SVR) model separately, and use the five-fold cross-validation method to select the optimal power m. The result of the machine learning evaluation is shown in Fig. 3a. It can be seen that when the power $m = 3$, the mean square error is the smallest, which is 0.0695. Based on this, we choose $m = 3$ as the power of the DCD to provide an efficient data set for the machine learning model.

After the machine learning data set is ready, we draw the learning curve of the SVR model, as shown in Fig. 3b. It can be seen from the figure that as the sample size increases, the mean square error of the model in the training set decreases progressively, which indicates that the prediction accuracy of the model in the test set is getting higher and higher. It is worth noting that when the number of samples is only about 500, the accuracy of the model is below 0.1, which fully proves the superiority of the feature.

Then we further use grid search to adjust the hyper-parameters of the SVR model on the 800 sample training set. The five-fold cross-validation result of the optimized model on the training set is shown in Fig. 3c. The root means square error between the calculated value of DFT and the predicted value of 800 SVR models is 0.130 eV. Then, we use the trained model to predict a test set of 100 samples, and the root means square deviation between the true value and the predicted value is 0.131 eV. Fig. 3d shows the relative error percentage distribution of the model on 800 samples. The error distribution within ±20% accounts for about 87.9%, the error here can be reduced by expanding the dataset. The above results reflect the accuracy of the model prediction and at the same time prove the feasibility of using the DCD-based machine learning model to evaluate the catalytic performance of the surface active sites of amorphous alloys.

After training the SVR model, we densely sampled 46,000 adsorption sites on the upper and lower surfaces of $Pt_{84}@Pd_{140}Ni_{140}Cu_{140}P_{140}$, and used the SVR model to predict the ΔG_H of H adsorption sites. Inspired by the distance contribution descriptor, we screened 5096 adsorption sites to explore the relationship between H-metal (Pt, Pd, …) distance and ΔG_H, and analyze the H-metal bonding configurations (on-site, bridge, hollow) as shown in Fig. 4. As can be seen from the scatter plot in Fig. 4a, in the region of $1.0 < D_{H\text{-}Pt} < 2.0$ Å, the scatter plot takes on a parabolic shape, indicating that the H atoms in this region are mainly distributed on-site of Pt (Fig. 4c). The adsorption potential energy of H atoms is mainly affected by Pt atoms [38–40], so the energy of the H adsorption site is parabolically shaped. In the region of $2.0 < D_{H\text{-}Pt} < 2.5$ Å, the coexistence of parabolic tails and disordered scatter can be seen, and the H-metal bonding configuration is mainly the bridge or hollow bonding among H, Pt and other metals (Pd shows more favorable in Figs. 4b, d and e). When $D_{H\text{-}Pt} > 2.5$ Å, it can be seen that the region exhibits a disordered scatter distribution, which indicates without the

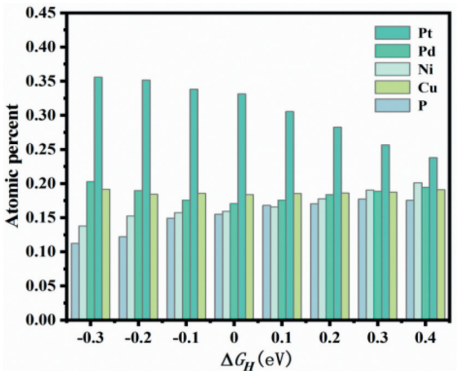

Fig. 5. Atomic statistical percentages of H adsorption sites in different ΔG_H intervals.

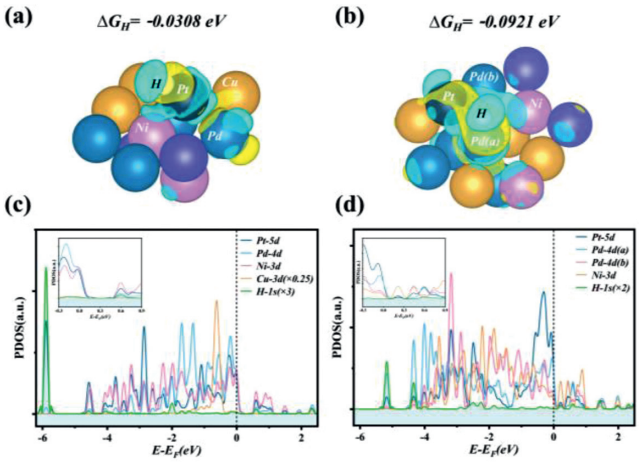

Fig. 6. The isosurface of charge difference before and after H atom adsorption on (a) Pt surface and (b) substrate surface. Yellow and cyan areas denote the charge accumulation and charge depletion, respectively. The projected state density of H atom adsorption sites in the (c) Pt surface and (d) substrate surface. The insets in (c, d) are the PDOS near the Fermi level.

influence of Pt-H, the H-bonding with other metals has a random distribution of ΔG_H.

Fig. 4b shows the H-metal distance contribution analysis as the function of ΔG_H. We add up the distance contribution value (DCD) of atoms of the same element in the cluster, an index ($D_{\text{contribute}}$) that can measure the size of the distance between H atoms and each element, which is defined as:

$$D_{\text{contribute}} = \sum_{i=1}^{n} DCD_i,\ i = 1,\ 2,\ 3, \ldots, n \tag{4}$$

where n represents the number of atoms of the same element in the adsorbed cluster. Here, the power of DCD is 3. It should be noted that the larger the $D_{\text{contribute}}$ value, the closer the distance between atoms. Then, we count the cases of $D_{\text{contribute}}$ in each ΔG_H interval (−0.25 to 0.45 eV), and the results are shown in Fig. 4b. When the Pt-H distance decreases, the ΔG_H of the adsorption site gradually decreases; when the Pd–H, Ni–H distance decreases, the ΔG_H of the adsorption site gradually increases; for Cu atoms and P atoms, the $D_{\text{contribute}}$ values are at low levels in different energy intervals, indicating that they have little effect on the ΔG_H of the adsorption site. In summary, the main factors affecting the catalytic performance of the adsorbed clusters are Pt, Pd and Ni atoms, which agrees well with experimental results [10]. Pt atoms are beneficial to reduce the ΔG_H of H adsorption clusters, while Pd and Ni atoms are beneficial for increasing the ΔG_H of H adsorption clusters. They jointly regulate the catalytic activity of adsorption clusters.

Considering the H-metal bonding configurations (on-site, bridge, hollow), we screened out 11,752 active sites with ΔG_H ranging from −0.35 eV to 0.45 eV among 46,000 adsorption sites. Then its atomic percentage in each energy interval was calculated, and the results are shown in Fig. 5. As the Pt atomic percentage gradually decreases, the ΔG_H of the active site gradually increases; in the local range of the energy interval −0.05 eV to 0.45 eV, as the Pd, Ni, and P atomic ratio increases, the ΔG_H of the active site gradually increases; for Cu atoms, there is no obvious trend in the atomic ratio as the energy interval increases. The above results are consistent with Fig. 4b. To obtain the atomic ratio of the best catalytic performance, we calculated the atomic ratio of ΔG_H between −0.05 and 0.05, which resulted in Pt:Pd:Ni:Cu:P = 0.33:0.17:0.155:0.16:0.185.

To gain a deeper understanding of the catalytic mechanism of H atom adsorption on the surface of Pt atoms and the substrate surface, we selected the adsorption sites with ΔG_H close to 0 in these two adsorption cases, and plotted the differential charge density map, as shown in Fig. 6. We mainly focus on the nearest neighbors of H atoms because they interact with H the strongest. Fig. 6a shows the adsorption site on the surface of Pt atoms. It can be seen that the charge density between H atoms and Pt atoms is high, while the charge density between H atoms and other coordination atoms is low, indicating that there is a strong interaction between H atoms and Pt atoms. Fig. 6b shows the adsorption site on the surface of the substrate. It can be seen that the charge density between H atoms and Pt, Pd and Ni atoms is very high, indicating that there is a strong interaction between them. To further confirm the contribution of the local atomic environment, we calculated the projected density of states of H atoms and their coordinating atoms in the adsorption sites in Figs. 6a and b.

Fig. 6c shows the H atom on the surface of the Pt atom. There are obvious resonance peaks between the s orbital of the H atom and of the Pt 5d orbital and Pd 4d orbital atoms, thereby forming a bond state at −2 eV. At the energy of −6 eV, the density of states of the Pt atom is larger, indicating that the Pt atom has a stronger binding force to the H atom. Fig. 6d shows the H atom on the surface of the substrate. There are obvious resonance peaks between the s orbital of the H atom and d orbital of the Pt, Pd(a), Pd(b) and Ni atoms, thus forming a bond state below −2 eV. Near the energy of −5 eV and the Fermi level, the density of states of Pt, Pd(a) and Ni atoms are larger, indicating that Pt, Pd and Ni atoms have the stronger binding force to H atoms. When H atoms are adsorbed on the surface of Pt, it is mainly because the Pt atoms improve the adsorption of H atoms. When H atoms are adsorbed on the substrate surface, Pt, Pd and Ni atoms can improve the adsorption of H atoms. In conclusion, Pt, Pd and Ni atoms can improve the adsorption of H atoms.

In summary, we used density functional theory (DFT) combined with machine learning to accurately predict the ΔG_H of 46,000 adsorption sites on the surface of an amorphous alloy (Pt@PdNiCuP), and research the factors affecting the catalytic activity. The results show that Pt, Pd, and Ni are the main elements that affect catalytic activity. Among them, Pt is beneficial to reduce the ΔG_H of the system, while Pd and Ni increase the ΔG_H of the system. In addition, in the energy interval −0.05 to 0.05 eV, we get the atomic ratio of the best catalytic performance (Pt:Pd:Ni:Cu:P = 0.33:0.17:0.155:0.16:0.185). Finally, through the projected density of states analysis, it is further indicated that the d orbitals of Pt, Pd, and Ni atoms mainly affect the catalytic performance. Our research strategy provides a new idea for the study of amorphous alloy catalysts, which can be extended to other promising catalytic materials.

Declaration of competing interest

The authors declare that they have no known competing financial interests or personal relationships that could have appeared to influence the work reported in this paper.

Acknowledgments

The supports of this work by the National Natural Science Foundation (Nos. 52275565 and 62104155) of China, Natural Science Foundation of Guangdong Province (No. 2022A1515011667) and Guangdong Kangyi Special Fund (No. 2020KZDZX1173).

Supplementary materials

Supplementary material associated with this article can be found, in the online version, at doi:10.1016/j.cclet.2022.107833.

References

[1] D. Suman, J. Ind. Eng. Chem. 20 (2014) 1148–1156.
[2] H. Chen, Y. Zhou, W. Guo, et al., Chin. Chem. Lett. 33 (2022) 1831–1840.
[3] X. Zou, Y. Zhang, Chem. Soc. Rev. 44 (2015) 5148–5180.
[4] V.S. Thoi, Y. Sun, J.R. Long, C.J. Chang, Chem. Soc. Rev. 42 (2013) 2388–2400.
[5] X. Yang, W. Xu, S. Cao, et al., Appl. Catal. B: Environ. 246 (2019) 156–165.
[6] F. Chu, K. Wu, Y. Meng, et al., J. Non Cryst. Solids 566 (2021) 120831.
[7] S. Ju, J. Feng, P. Zou, et al., J. Mater. Chem. A 8 (2020) 3246–3251.
[8] K. Wang, Y. Si, Z. Lv, et al., Int. J. Hydrog. Energy 45 (2020) 2504–2512.
[9] W. Teng, Z. Sun, J. Xie, et al., Front. Chem. 8 (2020) 552795.
[10] Y. Yan, C. Wang, Z. Huang, et al., J. Mater. Chem. A 9 (2021) 5415–5424.
[11] R.O. Jones, Rev. Mod. Phys. 87 (2015) 897–923.
[12] J.K. Norskov, F. Abild-Pedersen, F. Studt, T. Bligaard, Proc. Natl. Acad. Sci. U. S. A. 108 (2011) 937–943.
[13] W. Song, J. Wang, L. Fub, et al., Chin. Chem. Lett. 32 (2021) 3137–3142.
[14] P. Chen, B. Zhang, X. Gu, W. Lic, Chin. J. Chem. Phys. 32 (2019) 437–443.
[15] Z. Li, S. Wang, W. Chin, et al., J. Mater. Chem. A 5 (2017) 24131–24138.
[16] B.R. Goldsmith, J. Esterhuizen, J. Liu, et al., AIChE J. 64 (2018) 2311–2323.
[17] R.B. Wexler, J.M.P. Martirez, A.M. Rappe, J. Am. Chem. Soc. 140 (2018) 4678–4683.
[18] J. Noh, S. Back, J. Kim, Y. Jung, Chem. Sci. 9 (2018) 5152–5159.
[19] X. Zhu, J. Yan, M. Gu, et al., J. Phys. Chem. Lett. 10 (2019) 7760–7766.
[20] T. Williams, K. McCullough, J.A. Lauterbach, Chem. Mater. 32 (2019) 157–165.
[21] X. Sun, J. Zheng, Y. Gao, et al., Appl. Surf. Sci. 526 (2020) 146522.
[22] C. Deng, Y. Su, F. Li, et al., J. Mater. Chem. A 8 (2020) 24563–24571.
[23] X. Zhou, J. Zhu, Y. Wu, et al., Acta Mater. 224 (2022) 117535.
[24] T.A.A. Batchelor, J.K. Pedersen, S.H. Winther, et al., Joule 3 (2019) 834–845.
[25] X. Mao, L. Wang, Y. Xu, et al., NPJ Comput. Mater. 7 (2021) 46.
[26] W.A. Saidi, W. Shadid, G. Veser, J. Phys. Chem. Lett. 12 (2021) 5185–5192.
[27] T. Wu, M.L. Stone, M.J. Shearer, et al., ACS Catal. 8 (2018) 1143–1152.
[28] A Soon, M Todorova, B Delley, C Stampfl, Phys. Rev. B 73 (2006) 165424.
[29] J.P. Perdew, K. Burke, M. Ernzerhof, Phys. Rev. Lett. 77 (1996) 3865–3868.
[30] G. Kresse, J. Furthmuller, Comput. Mater. Sci. 6 (1996) 15–50.
[31] B. Hinnemann, P.G. Moses, J. Bonde, et al., J. Am. Chem. Soc. 127 (2005) 5308–5309.
[32] P. Liu, J.A. Rodriguez, J. Am. Chem. Soc. 127 (2005) 14871–14878.
[33] H. Wu, H. Huang, J. Zhong, et al., Nanoscale 11 (2019) 12210–12219.
[34] R. PARSON, J. Chem. Soc. Faraday Trans. 54 (1957) 1053–1063.
[35] J.K. Norskov, T. Bligaard, A. Logadottir, et al., J. Electrochem. Soc. 152 (2005) J23–J26.
[36] Z.L. Lu, Z.W. Chen, C.V. Singh, Matter 3 (2020) 1318–1333.
[37] F. Pedregosa, G. Varoquaux, A. Gramfort, et al., J. Mach. Learn. Res. 12 (2011) 2825–2830.
[38] K. Nobuhara, H. Nakanishi, H. Kasai, A. Okiji, J. Appl. Phys. 88 (2000) 6897–6901.
[39] S.C. Badescu, P. Salo, T. Ala-Nissila, et al., Phys. Rev. Lett. 88 (2002) 136101.
[40] R.A. Olsen, S.C. Badescu, S.C. Ying, E.J. Baerends, J. Chem. Phys. 120 (2004) 11852–11863.